

Experimental test of the differential fluctuation theorem and a generalized Jarzynski equality for arbitrary initial states

Thai M. Hoang,^{1,*} Rui Pan,² Jonghoon Ahn,³ Jaehoon Bang,³ H. T. Quan,^{2,4,†} and Tongcang Li^{1,3,5,6,‡}

¹*Department of Physics and Astronomy, Purdue University, West Lafayette, IN 47907, USA*

²*School of Physics, Peking University, Beijing 100871, China*

³*School of Electrical and Computer Engineering,
Purdue University, West Lafayette, IN 47907, USA*

⁴*Collaborative Innovation Center of Quantum Matter, Beijing 100871, China*

⁵*Purdue Quantum Center, Purdue University, West Lafayette, IN 47907, USA*

⁶*Birck Nanotechnology Center, Purdue University, West Lafayette, IN 47907, USA*

(Dated: October 3, 2018)

Nonequilibrium processes of small systems such as molecular machines are ubiquitous in biology, chemistry and physics, but are often challenging to comprehend. In the past two decades, several exact thermodynamic relations of nonequilibrium processes, collectively known as fluctuation theorems, have been discovered and provided critical insights. These fluctuation theorems are generalizations of the second law, and can be unified by a differential fluctuation theorem. Here we perform the first experimental test of the differential fluctuation theorem, using an optically levitated nanosphere in both underdamped and overdamped regimes, and in both spatial and velocity spaces. We also test several theorems that can be obtained from it directly, including a generalized Jarzynski equality that is valid for arbitrary initial states, and the Hummer-Szabo relation. Our study experimentally verifies these fundamental theorems, and initiates the experimental study of stochastic energetics with the instantaneous velocity measurement.

In the past two decades, there were significant developments in nonequilibrium statistical mechanics of small systems in which thermal fluctuation is influential [1]. The most prominent progresses are the discoveries of various fluctuation theorems (FT), which connect microscopic dynamics with thermodynamic behaviors [1]. These FT, such as the Jarzynski equality (JE) [2, 3] and the Crooks fluctuation theorem (CFT) [4, 5], reformulate the inequality of the second law into equalities, and reveal the universal laws that the fluctuating thermodynamic variables must obey in processes arbitrarily far from thermal equilibrium. As they are refinements of the second law on individual trajectories, they provide critical understandings of behaviors of biological systems at the single molecular level [3, 5–10] and nonequilibrium dynamics of a wide range of physical systems [11–28]. While JE and CFT are valid for processes far from thermal equilibrium, they require the initial state to be in a thermal equilibrium state.

In 2000, a differential fluctuation theorem (DFT) connecting the joint probabilities of entropy production and arbitrary generalized coordinates (e.g. position and velocity coordinates) was derived by Jarzynski [29]. An equivalent DFT for work was derived by Nobel laureate Karplus and his colleagues Maragakis and Spichty in 2008 [20]. It is remarkable that the DFT can unify various FT as long as detailed balance is not violated [20] (see Fig. S1 in the supplemental material for the relation between different fluctuation theorems [30]). The DFT also leads to a generalized Jarzynski equality (GJE) for arbitrary initial states [24]. Such ability is rooted from the fact that most FT originate from the same fundamental prin-

ciple: the microscopic reversibility connecting forward and reverse trajectories [1, 18, 24, 29, 31–33]. Testing the DFT and other FT would deepen our understanding of the second law and nonequilibrium physics, including dissipation [19], hysteresis [34], and irreversibility [35]. In order to test the DFT at its desired level of detail, we need large statistics and the ability to track individual trajectories of a stochastic process in the phase space [20], which requires the measurement of instantaneous velocities of Brownian motion [36].

In this work, we experimentally test the differential fluctuation theorem [20, 29] using an optically levitated nanosphere which can be trapped in air continuously for weeks for acquiring large sets of data. Our ultrasensitive optical tweezer can measure both instantaneous position and instantaneous velocity [36] of a levitated nanosphere to test DFT. Over one million experimental cycles per setting ($\sim 10^{10}$ position data points per setting with a 10 MHz acquisition rate) provide sufficient statistics to validate the DFT at its desired level of detail, e.g., testing DFT for nonequilibrium processes connecting two points in the position-velocity space [20]. Several fluctuation theorems, including the JE [2, 3], the CFT [4, 5], the Hummer-Szabo relation (HSR) [6–8], the GJE [19, 24, 31], the extended fluctuation relation (EFR) [9, 10], and the fluctuation theorem for ligand binding (FTLB) [37] can be unified by the DFT [18, 24, 31, 32]. We have also tested several such theorems. In our experiment, the air pressure can be adjusted to test these theorems in both underdamped and overdamped regimes. This study demonstrates a powerful approach applicable in exploring a wide range of nonequilibrium systems [3, 5–

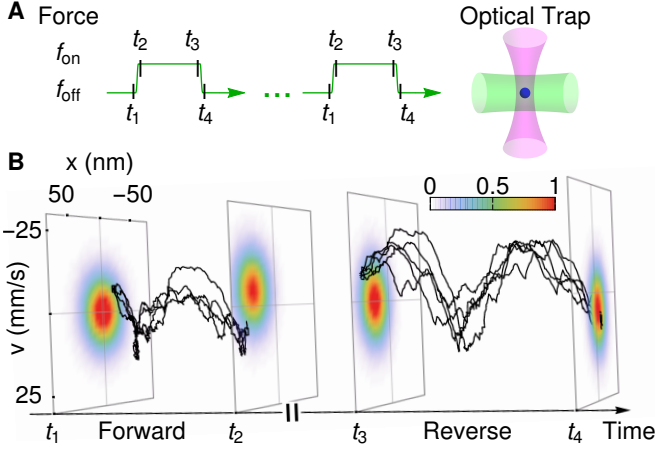


FIG. 1. **A**, Experimental scheme. A silica nanosphere (blue sphere) is trapped in an optical tweezer formed by a focused 1550-nm laser beam (magenta). A series of 532-nm laser pulses (green) exerts an optical force on the nanosphere to drive nonequilibrium processes. Within each pulse, an optical force is rapidly ramped from f_{off} at time t_1 to f_{on} at time t_2 during the forward process (green pulse). The reverse process from time t_3 to t_4 is the time-reversed correspondence of the forward process. **B**, An example of experimental data. Vertical slides represent the measured time snapshots of the probability distributions at times t_1 , t_2 , t_3 , and t_4 as illustrated in **A**. Black curves represent experimental phase-space trajectories during forward processes initialized at (x_1, v_1) and finalized at (x_2, v_2) , and during reverse processes initialized at the $(x_2, -v_2)$ and finalized at $(x_1, -v_1)$. Here $x_1 = -19$ nm, $x_2 = 55$ nm, $v_1 = -7$ mm/s, and $v_2 = 7$ mm/s. The nanosphere is levitated in air at 50 torr, and $f_{\text{off}} = 0$, $f_{\text{on}} = 340$ fN.

13, 15, 16] since a complete description of the stochastic system includes the information of both position and velocity.

Our experiments are carried out using a silica nanosphere levitated by a 1550 nm optical tweezer (Fig. 1A) [38]. The nonequilibrium processes are controlled by a force parameter f which is an optical force exerted on the nanosphere by a 532-nm laser beam. In a forward process, the optical force is ramped from f_{off} at time t_1 to f_{on} at time t_2 . The reverse process is from t_3 to t_4 . The DFT connects the forward and reverse processes as [20, 29]:

$$P_R(-W, b^* \rightarrow a^*) / P_F(W, a \rightarrow b) = e^{-\beta(W - \Delta F)}, \quad (1)$$

where a , b can be arbitrary generalized coordinates. In our work, a and b denote the position (x) and/or velocity (v) coordinate of a levitated nanosphere, e.g., a can be x , or v , or (x, v) . $P_F(W, a \rightarrow b)$ is the forward joint probability of performing nonequilibrium work W for those trajectories starting from a and ending at b , and $P_R(-W, b^* \rightarrow a^*)$ is the reverse joint probability. The work distribution $P_F(W)$ can be obtained by integrating $P_F(W, a \rightarrow b)$ over a and b . The asterisk (*)

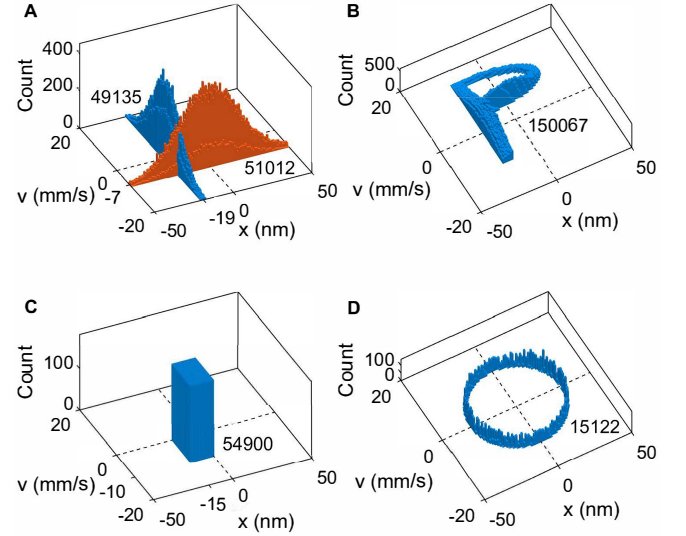


FIG. 2. Examples of arbitrary nonequilibrium initial states of trajectory ensembles prepared by an information-based method. **A**, Nonequilibrium initial states with narrow distributions in position or velocity. **B**, An exotic nonequilibrium state with a P-shaped distribution in phase space. **C**, Uniform distribution within a rectangle (-15 nm $< x < 0$, -10 mm/s $< v < 0$) in the phase space. **D**, A microcanonical ensemble with the energy shell $1.3k_B T < E < 1.35k_B T$. The number of experimental trajectories started from each nonequilibrium initial state is labeled next to its distribution.

denotes a reversal of the velocity components of a or b . $\Delta F = -(f_{\text{on}}^2 - f_{\text{off}}^2)/(2k)$ is the free energy difference between the equilibrium states of the optical forces f_{on} and f_{off} . Here k is the trap stiffness. $\beta = 1/(k_B T)$, where k_B is the Boltzmann constant, and $T = 296$ K is the room temperature.

To test the DFT in detail, over one million experimental forward-reverse cycles (500 μ s/cycle) are performed for a given irreversible setting. Their distributions in the position-velocity space are shown in Fig. 1B. The driving optical forces significantly shift the distributions away from the undriven ones. Black curves in Fig. 1B are a few examples of measured trajectories evolving from a given point to a different point in the phase space during forward (or reverse) processes. Due to thermal fluctuation, it is not possible to have two trajectories starting from exactly the same point in the phase space. Here we use (x, v) to represent points within $(x \pm \frac{\sigma_x}{11}, v \pm \frac{\sigma_v}{11})$, where σ_x and σ_v are the standard deviations of the position and velocity distributions, respectively.

Based on our large sets of experimental data and our ability to measure both the instantaneous velocity and position of a nanoparticle, we develop an efficient method to prepare arbitrary nonequilibrium initial states by conditionally selecting trajectories that start from the desired initial states. Some examples of arbitrary nonequilibrium initial states prepared by our information-based

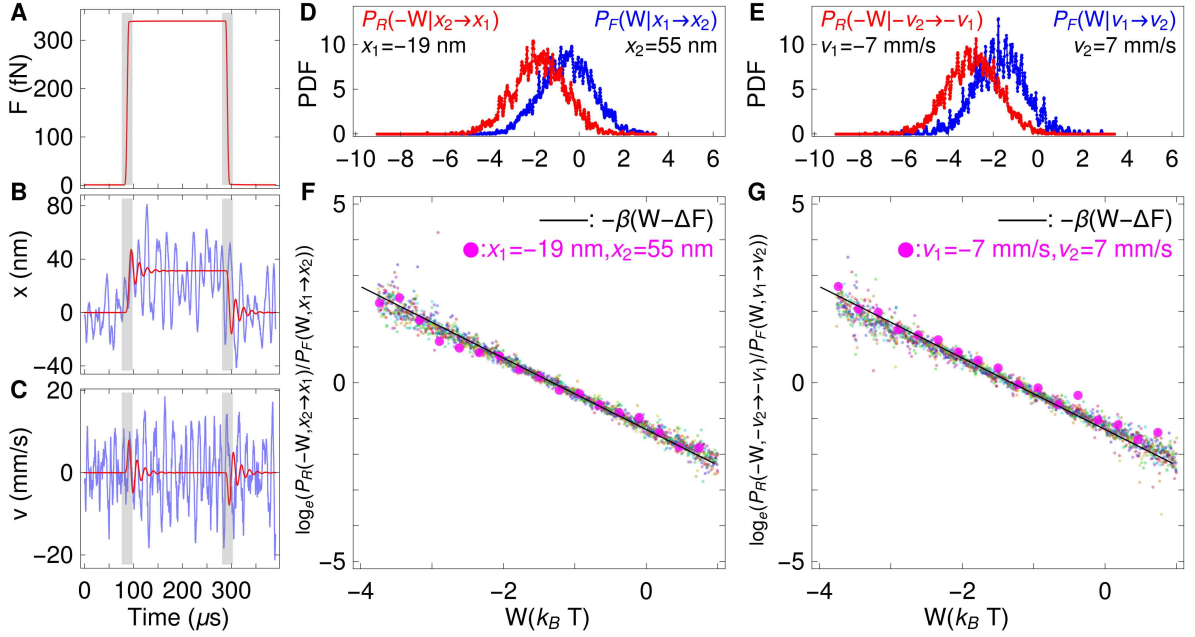


FIG. 3. Testing the differential fluctuation theorem in the underdamped regime. **A**, Optical force. **B-C**, Measured position and velocity trajectories. A single trajectory is shown in blue, and the averaged trajectory of over one million trajectories is shown in red. The gray shaded regions in **A-C** denote the forward and reverse intervals, respectively. It takes roughly $4.6 \mu\text{s}$ for the optical force strength to switch from 10% to 90% level. **D**, An example of probabilities $P_F(W|x_1 \rightarrow x_2)$ and $P_R(-W|x_2 \rightarrow x_1)$ in position coordinate. **E**, An example of probabilities $P_F(W|v_1 \rightarrow v_2)$ and $P_R(-W|-v_2 \rightarrow -v_1)$ in velocity coordinate. The label of horizontal axis in **D** and **E** is $W(k_B T)$. **F**, **G** Testing the DFT in position and velocity spaces. The small markers with different colors represent measurements of $\log_e \frac{P_R(-W, x_2 \rightarrow x_1)}{P_F(W, x_1 \rightarrow x_2)}$ and $\log_e \frac{P_R(-W, -v_2 \rightarrow -v_1)}{P_F(W, v_1 \rightarrow v_2)}$ for 121 different $\{x_1, x_2\}$ and $\{v_1, v_2\}$ combinations, respectively. The big magenta markers are results for parameters shown in **D** and **E**, respectively. The black lines represent $-\beta(W - \Delta F)$.

method are shown in Fig. 2. They are used to test the DFT and the GJE for arbitrary initial states.

Fig. 3 shows our experimental results of testing DFT with a 209-nm-radius nanoparticle in the underdamped regime (see supplemental online material for more information [30]). The optical force (Fig. 3A) is monitored using a fraction of the 532-nm laser split from the main beam. Fig. 3B-C show the dynamic evolution of the nanoparticle in the position and velocity coordinates, respectively. Since the irreversible ramps ($\sim 4.6 \mu\text{s}$) are faster than the velocity ($\sim 8.6 \mu\text{s}$) and position ($\sim 100 \mu\text{s}$) relaxation times, the nanoparticle is far from thermal equilibrium when the ramps finish.

With the acquired position, velocity and force data, the DFT is ready to be tested. The DFT in Eq. 1 can be rewritten in the position coordinate as, $\frac{P_R(-W, x_2 \rightarrow x_1)}{P_F(W, x_1 \rightarrow x_2)} = \frac{P_R(x_2 \rightarrow x_1)}{P_F(x_1 \rightarrow x_2)} \frac{P_R(-W|x_2 \rightarrow x_1)}{P_F(W|x_1 \rightarrow x_2)}$ [20]. Here $P_F(x_1 \rightarrow x_2)$ is the probability of having a forward trajectory going from x_1 to x_2 , and $P_R(x_2 \rightarrow x_1)$ is the probability of a reverse trajectory going from x_2 to x_1 . These quantities can be calculated using the distributions illustrated in the Fig. 1B. They are essentially equivalent to the number of forward (reverse) trajectories going from x_1 to x_2 (x_2 to x_1). $P_F(W|x_1 \rightarrow x_2)$ is the probability of

performing work W for those forward trajectories going from x_1 to x_2 , and $P_R(-W|x_2 \rightarrow x_1)$ is the reverse probability (Fig. 3D). Similarly, Fig. 3E shows examples of $P_F(W|v_1 \rightarrow v_2)$ and $P_R(-W|-v_2 \rightarrow -v_1)$ in the velocity coordinate. The minus sign ($-$) in the velocity space is due to the time reversal symmetry of the reverse process. Here irreversible work is calculated as $W = -\sum_{i=1}^{n-1} (f_{i+1} - f_i)(x_i + x_{i+1})/2$ for n successive position and force measurements. This formula is obtained using the Hamiltonian, $H = \frac{1}{2}kx^2 - fx + \frac{1}{2}mv^2$, and the work definition $W = \int_0^\tau dt \dot{f}(t) \frac{\partial H}{\partial f}$ during a ramp period τ [2].

The DFT is tested in detail using 121 different initial-final combinations in the position and velocity coordinates uniformly distributed in $(\pm\sigma_x, \pm\sigma_v)$. Fig. 3F shows that the left hand side, $\frac{P_R(-W, x_2 \rightarrow x_1)}{P_F(W, x_1 \rightarrow x_2)}$, agrees well with the right hand side, $e^{-\beta(W - \Delta F)}$, of the DFT in Eq. 1. Here $e^{-\beta(W - \Delta F)}$ is a function of the work variable W . The free energy difference can be calculated as $\Delta F = -1.3 k_B T$ with $f_{\text{off}}/f_{\text{on}} = 0/340 \text{ fN}$ (Fig. 3A). Similarly, we can verify the DFT in the velocity coordinate (Fig. 3G). Data points also distribute closely to the curves $e^{-\beta(W - \Delta F)}$. Thus our data agree with the DFT well in position and velocity coordinates simultaneously.

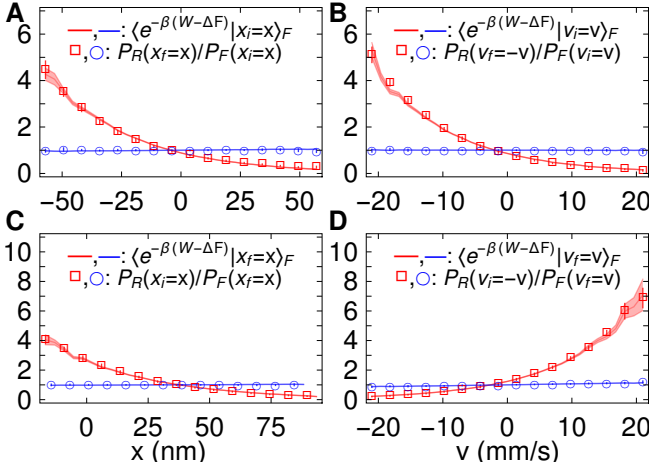


FIG. 4. Testing fluctuation theorems in the underdamped regime. **A, B**, Testing GJE in position and velocity spaces for a fast ramp (red, 4.6 μ s from 10% to 90% levels), and a slow ramp (blue, 40 μ s from 10% to 90% levels). Markers represent the measured $P_R(x_f = x)/P_F(x_i = x)$ and $P_R(v_f = -v)/P_F(v_i = v)$ in position and velocity spaces, respectively. **C, D**, Testing HSR in position and velocity spaces for a fast ramp (red) and a slow ramp (blue). Markers represent the measured $P_R(x_i = x)/P_F(x_f = x)$ and $P_R(v_i = -v)/P_F(v_f = v)$ in position and velocity spaces, respectively. The errorbars of $P_R(x)/P_F(x)$ and $P_R(-v)/P_F(v)$ represent the standard deviation of the measurements for 20 equal divisions in each subset x and v , respectively. The markers represent their mean values. In **A–D**, the shaded line represent $\langle e^{-\beta(W-\Delta F)} \rangle$, where its thickness represents the uncertainty of 600 work (Joule) calibrations.

Our experimental data can also test other fluctuation theorems which are direct integrations of the DFT [30]. Integrating the Eq. 1 over W and b , we obtain the GJE for delta initial distributions in the position or velocity coordinates ($a = x$ or $a = v$) [19, 24, 31],

$$\begin{aligned} \langle e^{-\beta(W-\Delta F)} | x_i = x \rangle_F &= P_R(x_f = x)/P_F(x_i = x), \\ \langle e^{-\beta(W-\Delta F)} | v_i = v \rangle_F &= P_R(v_f = -v)/P_F(v_i = v). \end{aligned} \quad (2)$$

Here $P_F(x_i = x)$ is the probability that a forward trajectory *initializes* at x , and $P_R(x_f = x)$ is the probability that a reverse trajectory *finalizes* at x . We use subscripts “ i ” and “ f ” to denote “initial” and “final” respectively. Similarly, $P_F(v_i = v)$ and $P_R(v_f = -v)$ are the probabilities in the velocity coordinate. They are proportional to the number of trajectories *initialized* (*finalized*) at x or v (Fig. 2A). The value $\langle e^{-\beta(W-\Delta F)} | x_i = x \text{ (or } v_i = v) \rangle_F$ is averaged over all forward trajectories initialized at x or v in the position or velocity coordinates. The data agree well with the GJE as shown in Fig. 4A,B. For slow ramps, the measured $\langle e^{-\beta(W-\Delta F)} | x_i \text{ (or } v_i) \rangle_F$ stays closely to 1, which is the result of a reversible process. However, for fast (irreversible) ramps, the values of $\langle e^{-\beta(W-\Delta F)} | x_i \text{ (or } v_i) \rangle_F$ diverge away from 1, so the GJE is needed to explain our observations.

Initial state	Thermal equilibrium	P-shaped state (Fig. 2B)	Uniform distribution (Fig. 2C)	Microcanonical ensemble (Fig. 2D)
lhs	1.02 ± 0.02	0.92 ± 0.02	1.42 ± 0.03	1.08 ± 0.02
rhs	1	0.90	1.42	1.07

TABLE I. Test of the GJE for arbitrary initial states. The thermal equilibrium state and three representative nonequilibrium initial states shown in Fig. 2B, 2C, 2D are chosen for the test. The second and third rows show the data of the lhs and rhs of Eq. 4 for each initial state, respectively.

Similarly, integrating Eq. 1 over W and a leads to the HSR [30] in the position and velocity spaces ($b = x$ or $b = v$) [6, 19, 20],

$$\begin{aligned} \langle e^{-\beta(W-\Delta F)} | x_f = x \rangle_F &= P_R(x_i = x)/P_F(x_f = x), \\ \langle e^{-\beta(W-\Delta F)} | v_f = v \rangle_F &= P_R(v_i = -v)/P_F(v_f = v). \end{aligned} \quad (3)$$

Here $\langle e^{-\beta(W-\Delta F)} | x_f = x \text{ (or } v_f = v) \rangle_F$, $P_F(x_f = x)$, and $P_R(x_i = x)$ are denoted using the same conventions as in the GJE in Eq. 2. The data agree well with the HSR for both fast (irreversible) ramps and slow (reversible) ramps as shown in Fig. 4C,D.

Integrating Eq. 2 over initial phase space points with an arbitrary initial distribution, one obtains the GJE for arbitrary initial states proposed in Ref. [24]

$$\begin{aligned} \langle e^{-\beta(W-\Delta F)} \rangle_{P_{ini}(x_i, v_i)} &= \\ \int \frac{P_R(x_f = x, v_f = -v)}{P_F(x_i = x, v_i = v)} P_{ini}(x_i = x, v_i = v) dx dv, \end{aligned} \quad (4)$$

where $P_{ini}(x_i, v_i)$ indicates an arbitrary initial distribution in phase space. We test Eq. 4 for the thermal equilibrium initial state and three representative nonequilibrium initial states as shown in Fig. 2B, 2C, 2D. The results are shown in TABLE I. The left hand side (lhs) and right hand side (rhs) of Eq. 4 agree well with each other within the experimental uncertainty.

With our experimental data we can test JE [2] and CFT [4] with high precision. The results are shown in Fig. S2 in the supplemental material [30]. For completeness, we also tested the DFT in the overdamped regime ($a = x_1$ and $b = x_2$) where the velocity relaxes to equilibrium much faster than other processes. As shown in Fig. S3 in the supplemental material [30], our experimental data show good agreements with HSR [6], the DFT [20], and the GJE [19, 24]. Overall, the differential fluctuation theorem unifies many existing fluctuation theorems [9, 10, 18, 24, 31, 32, 37], such as JE, CFT, HSR, GJE, EFR, and FTLB, and is arguably the most detailed fluctuation theorem that can be tested experimentally. The DFT can also improve free energy calculations [20]. Our experimental results validate the DFT [20] well in both underdamped and overdamped regimes. Our work

deepens our understanding of the second law to an unprecedentedly detailed level. It initiates the experimental study of stochastic thermodynamics with instantaneous velocity measurements, and may shed new light on our understanding of the origin of time's arrow [34]. Once cooled to the quantum regime, a levitated nanosphere in vacuum can be used to investigate quantum nonequilibrium thermodynamics in the mesoscopic regime [39]. This system can also be used to study effects of geometry in thermodynamic control [40].

T.L. acknowledges support from NSF under Grant No. PHY-1555035 and the Tellabs Foundation. H.T.Q. acknowledges support from the National Science Foundation of China under grants 11375012, 11534002, and The Recruitment Program of Global Youth Experts of China.

* Current address: Sandia National Laboratories, Albuquerque, NM 87123

† Corresponding author: htquan@pku.edu.cn

‡ Corresponding author: tcli@purdue.edu

- [1] C. Jarzynski, *Annu. Rev. Condens. Matter Phys.* **2**, 329 (2011).
- [2] C. Jarzynski, *Phys. Rev. Lett.* **78**, 2690 (1997).
- [3] J. Liphardt, S. Dumont, S. B. Smith, I. Tinoco, and C. Bustamante, *Science* **296**, 1832 (2002).
- [4] G. E. Crooks, *Phys. Rev. E* **60**, 2721 (1999).
- [5] D. Collin, F. Ritort, C. Jarzynski, S. B. Smith, I. Tinoco, and C. Bustamante, *Nature* **437**, 231 (2005).
- [6] G. Hummer and A. Szabo, *Proc. Natl. Acad. Sci.* **98**, 3658 (2001).
- [7] N. C. Harris, Y. Song, and C.-H. Kiang, *Phys. Rev. Lett.* **99**, 068101 (2007).
- [8] A. N. Gupta, A. Vincent, K. Neupane, H. Yu, F. Wang, and M. T. Woodside, *Nature Phys.* **7**, 631 (2011).
- [9] I. Junier, A. Mossa, M. Manosas, and F. Ritort, *Phys. Rev. Lett.* **102**, 070602 (2009).
- [10] A. Alemany, A. Mossa, I. Junier, and F. Ritort, *Nature Phys.* **8**, 688 (2012).
- [11] G. M. Wang, E. M. Seveck, E. Mittag, D. J. Searles, and D. J. Evans, *Phys. Rev. Lett.* **89**, 050601 (2002).
- [12] E. Trepagnier, C. Jarzynski, F. Ritort, G. E. Crooks, C. Bustamante, and J. Liphardt, *Proc. Natl. Acad. Sci.* **101**, 15038 (2004).
- [13] F. Douarche, S. Joubaud, N. B. Garnier, A. Petrosyan, and S. Ciliberto, *Phys. Rev. Lett.* **97**, 140603 (2006).
- [14] Y. Jun, M. Gavrilov, and J. Bechhoefer, *Phys. Rev. Lett.* **113**, 190601 (2014).
- [15] J. Gieseler, R. Quidant, C. Dellago, and L. Novotny, *Nat. Nanotechnol.* **9**, 358 (2014).
- [16] D. Y. Lee, C. Kwon, and H. K. Pak, *Phys. Rev. Lett.* **114**, 060603 (2015).
- [17] J. P. Pekola, *Nature Phys.* **11**, 118 (2015).
- [18] U. Seifert, *Phys. Rev. Lett.* **95**, 040602 (2005).
- [19] R. Kawai, J. M. R. Parrondo, and C. van den Broeck, *Phys. Rev. Lett.* **98**, 080602 (2007).
- [20] P. Maragakis, M. Spichty, and M. Karplus, *J. Phys. Chem. B* **112**, 6168 (2008).
- [21] M. Esposito and C. van den Broeck, *Phys. Rev. Lett.* **104**, 090601 (2010).
- [22] T. Sagawa and M. Ueda, *Phys. Rev. Lett.* **104**, 090602 (2010).
- [23] S. Toyabe, T. Sagawa, M. Ueda, E. Muneyuki, and M. Sano, *Nature Phys.* **6**, 988 (2010).
- [24] Z. Gong and H. T. Quan, *Phys. Rev. E* **92**, 012131 (2015).
- [25] V. Blickle, T. Speck, L. Helden, U. Seifert, and C. Bechinger, *Phys. Rev. Lett.* **96**, 070603 (2006).
- [26] I. A. Martinez, E. Roldan, L. Dinis, D. Petrov, J. M. R. Parrondo, and R. A. Rica, *Nature Phys.* **12**, 67 (2016).
- [27] A. Bérut, A. Petrosyan, and S. Ciliberto, *EPL* **103**, 60002 (2013).
- [28] J. V. Koski, V. F. Maisi, T. Sagawa, and J. P. Pekola, *Phys. Rev. Lett.* **113**, 030601 (2014).
- [29] C. Jarzynski, *J. Stat. Phys.* **98**, 77 (2000).
- [30] See Supplemental Material at [URL will be inserted by publisher] for the relation between various FT, the test of JE and CFT, the calibration method, and results in the overdamped regime.
- [31] G. E. Crooks, *Excursions in Statistical Dynamics* (PhD Thesis. University of California, Berkeley, 1999).
- [32] C. V. den Broeck, *Proceedings of the International School of Physics Enrico Fermi* **184**, 155 (2013).
- [33] U. Seifert, *Rep. Prog. Phys.* **75**, 126001 (2012).
- [34] E. H. Feng and G. E. Crooks, *Phys. Rev. Lett.* **101**, 090602 (2008).
- [35] A. Gomez-Marin, J. M. R. Parrondo, and C. Van den Broeck, *EPL* **82**, 50002 (2008).
- [36] T. Li, S. Kheifets, D. Medellin, and M. G. Raizen, *Science* **328**, 1673 (2010).
- [37] J. Camunas-Soler, A. Alemany, and F. Ritort, *Science* **355**, 412 (2017).
- [38] T. M. Hoang, J. Ahn, J. Bang, and T. Li, *Nat. Commun.* **7**, 12250 (2016).
- [39] Z.-q. Yin, A. A. Geraci, and T. Li, *Int. J. Mod. Phys. B* **27**, 1330018 (2013).
- [40] P. R. Zulkowski, D. A. Sivak, G. E. Crooks, and M. R. DeWeese, *Phys. Rev. E* **86**, 041148 (2012).

SUPPLEMENTAL MATERIAL

Relation between the differential fluctuation theorem and other fluctuation theorems

As discussed in the main text, the differential fluctuation theorem (DFT) [1, 2] unifies many existing fluctuation theorems, such as the Jarzynski equality (JE) [3, 4], the Crooks fluctuation theorem (CFT) [5, 6], the Hummer-Szabo relation (HSR) [7–9], the generalized Jarzynski equality (GJE) for the delta initial distribution [10] and a GJE for arbitrary initial states proposed in Ref. [11]. Fig. S1 shows the relation between the differential fluctuation theorem [1, 2] and other fluctuation theorems. The DFT is arguably the most detailed fluctuation theorem that can be tested experimentally. It originates from the microscopic reversibility of each trajectory. The CFT can be obtained by integrating the DFT over initial and final phase space points. The HSR can be obtained by integrating the DFT over initial phase space points and work. The GJE for delta initial distribution can be obtained by integrating the DFT over final phase space points and work. The JE can be obtained by integrating the CFT over work, or by integrating the HSR over final phase space points, or by integrating the generalized JE over initial phase space points with equilibrium distribution. We note that the CFT, the HSR, and the GJE can not be obtained directly from each other. The GJE for arbitrary initial distribution can be obtained by integrating the GJE for delta initial distribution

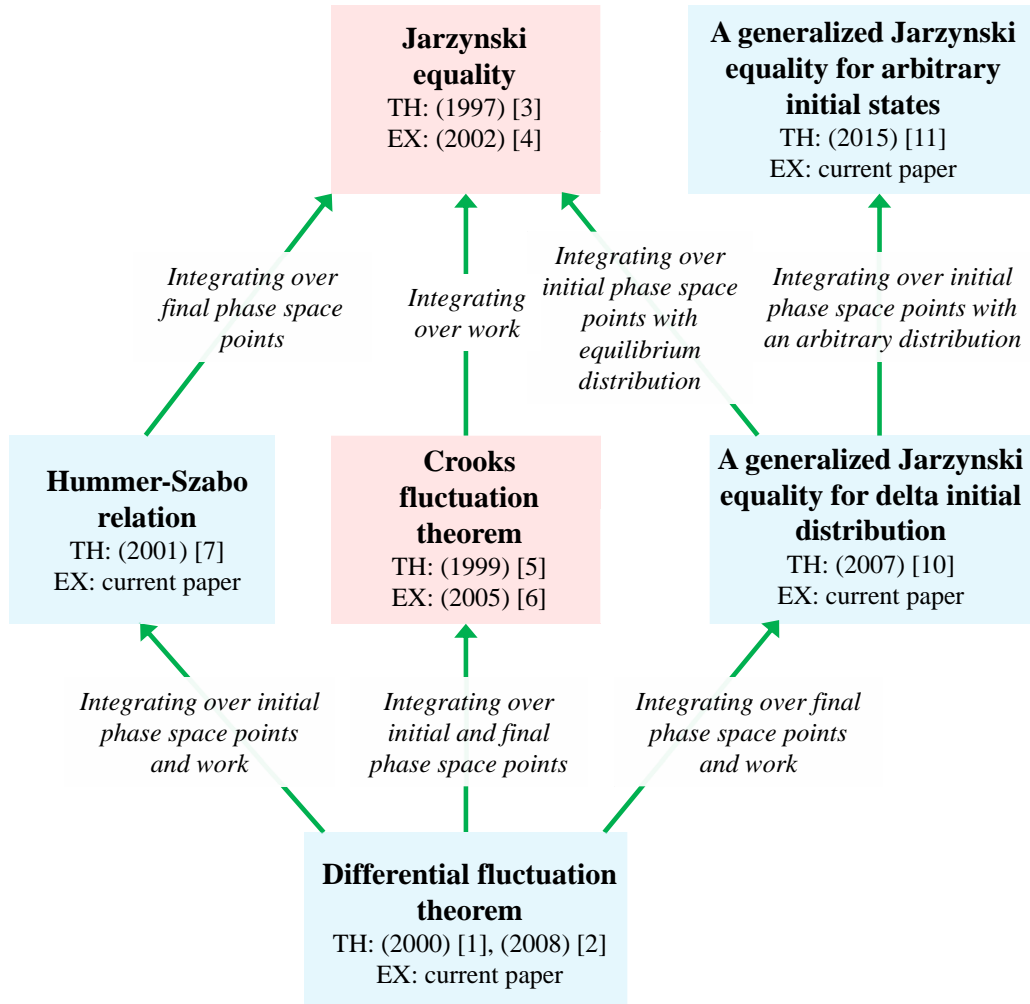


FIG. S1. Relation between the DFT and other FT. Here “TH” indicates “theory”, and “EX” indicates “experiment”. The number in a round bracket indicates the year in which the theory was proposed or the experiment was carried out, and the number in a square bracket indicates the reference source. It can be seen that the JE and the CFT have been tested experimentally before, which are highlighted with red background. The DFT, the HSR, the GJE for delta initial distribution and GJE for arbitrary initial states are tested in the current study. They are highlighted with blue background.

over initial phase space points with an arbitrary distribution. Among theorems listed in Fig. S1, the JE and the CFT have been tested experimentally before. While some particular cases of the GJE have been investigated elsewhere [10, 12–14], we used data of trajectory ensembles with arbitrary nonequilibrium initial states to perform the first experimental test of the generalized Jarzynski equality for arbitrary initial states proposed in [11].

Calibrations in underdamped regime

The particle position-velocity (x - v) is calibrated to SI units using the equipartition theorem, $k\langle x^2 \rangle = k_B T$. $k = (4/3)\pi r^3 \rho \Omega^2$ is the trap stiffness. The silica nanosphere has a mass density of $\rho = 1960 \text{ kg/m}^3$ (Bangs Laboratories). The power spectra and position autocorrelation function [15] yield a hydrodynamic radius $r = 209 \pm 9 \text{ nm}$ and a trapping frequency $\Omega/2\pi = 60.4 \pm 0.3 \text{ kHz}$. The optical force is calibrated using Hooke's law, $f = k\Delta x$, with Δx being the position displacement. The work (Joule) calibration is the product of the position and force calibrations.

The force data shown in Fig. 3A of the main text indicate that forward and reverse forces have good time-reversal symmetry with only $\sim 1\%$ difference in the area under the force curve. The particle velocity shown in Fig. 3C of the main text is calculated after binning 7 position points together to reduce the detection noise [16]. The nanosphere velocity has a signal-to-noise ratio of about 8.9. Here the signal-to-noise ratio of the nanosphere velocity is

$$v_{\text{SNR}} = \frac{\Delta v_{\text{nanosphere}}}{\Delta v_{\text{without nanosphere}}}. \quad (5)$$

$\Delta v_{\text{nanosphere}}$ is the standard deviation of the nanosphere velocity (signal), and $\Delta v_{\text{without nanosphere}}$ is the standard deviation of the velocity without nanosphere (noise).

Test of JE and CFT with a levitated nanoparticle in the underdamped regime

The JE [3] can be obtained by integrating Eq. 1 in the main text over a , b and W . Our experimental data show an excellent agreement with JE, $\langle e^{-\beta(W-\Delta F)} \rangle = 1.02 \pm 0.02$ (Fig. S2A). The CFT [5] can be obtained by integrating Eq. 1 in the main text over a and b , $P_R(-W)/P_F(W) = e^{-\beta(W-\Delta F)}$. The measurements of $\log_e(P_R(-W)/P_F(W))$ show an excellent agreement with a linear fit (Fig. S2B). The fit yields a linear slope of -0.99 ± 0.03 which agrees well with the theoretical slope of -1 .

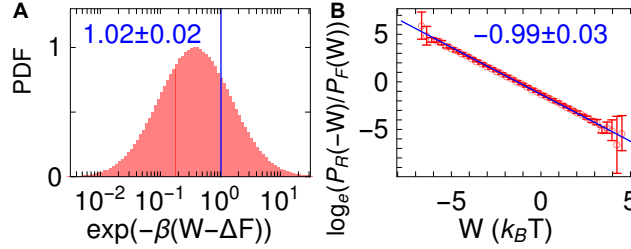


FIG. S2. Testing JE and CFT in the underdamped regime. **A**, Testing the JE using forward irreversible work, $\langle e^{-\beta(W-\Delta F)} \rangle = 1.02 \pm 0.02$ (vertical line). **B**, Testing the CFT. The slope of the linear fit yields a value -0.99 ± 0.03 . The errorbars and the uncertainty are due to the standard deviation of 600 work (Joule) calibrations.

Overdamped regime

For completeness, we also tested the DFT in the overdamped regime ($a = x_1$ and $b = x_2$) where the velocity relaxes to equilibrium much faster than other processes. So it is sufficient to measure the position only. A smaller nanosphere with a hydrodynamic radius $r = 145 \pm 5 \text{ nm}$ is levitated at a pressure of 760 torr. The trapping frequency is $\Omega = 76 \pm 3 (2\pi \cdot \text{kHz})$. The optical force profile and the position trajectories are shown in Fig. S3A,B. For a typical optical force, $f_{\text{off}}/f_{\text{on}} = 0/107 \text{ fN}$, the free energy difference is $\Delta F = -0.24 k_B T$. As shown in Fig. S3B, the nanosphere position is far from the equilibrium when the ramps finish. The experimental data show good agreements with the JE [3], the CFT [5], the GJE [11], HSR [7], and the DFT [2] as shown in Fig. S3C–G.

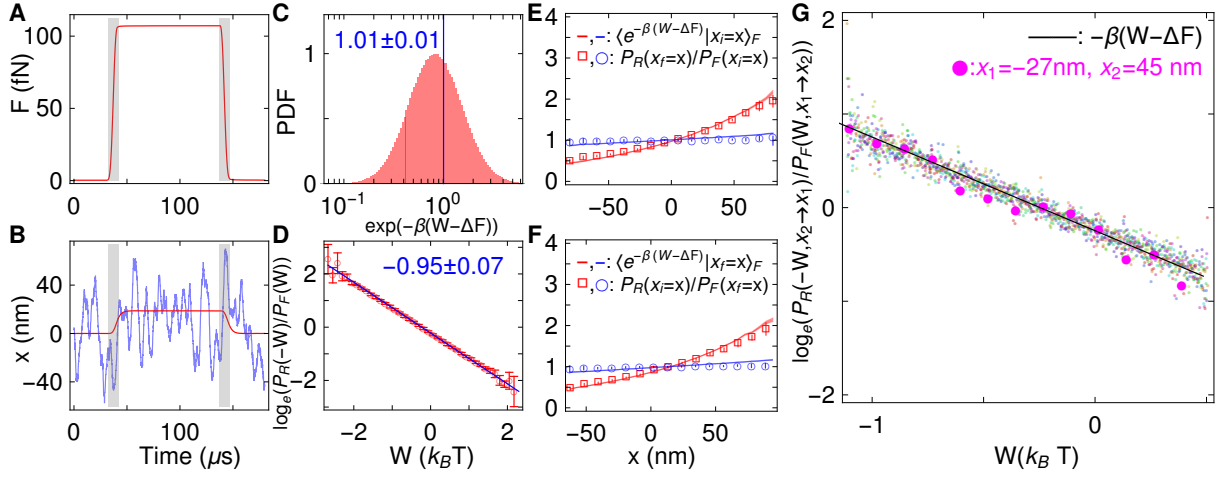


FIG. S3. Testing DFT and FT in the overdamped regime. **A**, The optical force. **B**, The average of over 1 million position trajectories is shown in red, and a single trajectory is shown in blue. **C**, Testing the JE using the forward irreversible work, $\langle e^{-\beta(W-\Delta F)} \rangle = 1.01 \pm 0.01$ (vertical line). **D**, Testing the CFT. The slope of the linear fit yields -0.95 ± 0.07 . In **C-D**, The errorbars and the uncertainty are the standard deviation of 600 work (Joule) calibrations. **E**, Testing the GJE in position space for a fast ramp (red, $4.8 \mu\text{s}$ from 10% to 90% level), and a slow ramp (blue, $62 \mu\text{s}$ from 10% to 90% level). **F**, Testing the HSR in position space for a fast ramp, and a slow ramp. In **E-F**, the shaded line represent $\langle e^{-\beta(W-\Delta F)} \rangle$, where its thickness represents the uncertainty due to 600 work (Joule) calibrations. The errorbars of $P_R(x_i=x)/P_F(x_f=x)$ represent the standard deviation of the measurements for 20 equal divisions within the range between $x - \frac{\sigma_x}{11}$ and $x + \frac{\sigma_x}{11}$. The markers represent their mean values. **G** Testing differential fluctuation theorem in position space. The small markers with different colors represent the measurements of $\log_e \frac{P_R(-W, x_2 \rightarrow x_1)}{P_F(W, x_1 \rightarrow x_2)}$ for 121 different combinations $\{x_1, x_2\}$. The large magenta markers illustrate data for the combination $\{-27 \text{ nm}, 45 \text{ nm}\}$. The black line represents $-\beta(W - \Delta F)$.

* Current address: Sandia National Laboratories, Albuquerque, NM 87123

† Corresponding author: htquan@pku.edu.cn

‡ Corresponding author: tcli@purdue.edu

- [1] C. Jarzynski, J. Stat. Phys. **98**, 77 (2000).
- [2] P. Maragakis, M. Spichty, and M. Karplus, J. Phys. Chem. B **112**, 6168 (2008).
- [3] C. Jarzynski, Phys. Rev. Lett. **78**, 2690 (1997).
- [4] J. Liphardt, S. Dumont, S. B. Smith, I. Tinoco, and C. Bustamante, Science **296**, 1832 (2002).
- [5] G. E. Crooks, Phys. Rev. E **60**, 2721 (1999).
- [6] D. Collin, F. Ritort, C. Jarzynski, S. B. Smith, I. Tinoco, and C. Bustamante, Nature **437**, 231 (2005).
- [7] G. Hummer and A. Szabo, Proc. Natl. Acad. Sci. **98**, 3658 (2001).
- [8] A. N. Gupta, A. Vincent, K. Neupane, H. Yu, F. Wang, and M. T. Woodside, Nature Phys. **7**, 631 (2011).
- [9] N. C. Harris, Y. Song, and C.-H. Kiang, Phys. Rev. Lett. **99**, 068101 (2007).
- [10] R. Kawai, J. M. R. Parrondo, and C. van den Broeck, Phys. Rev. Lett. **98**, 080602 (2007).
- [11] Z. Gong and H. T. Quan, Phys. Rev. E **92**, 012131 (2015).
- [12] T. Sagawa and M. Ueda, Phys. Rev. Lett. **104**, 090602 (2010).
- [13] A. Berut, A. Petrosyan, and S. Ciliberto, Europhys. Lett. **103**, 60002 (2013).
- [14] J. V. Koski, V. F. Maisi, T. Sagawa, and J. P. Pekola, Phys. Rev. Lett. **113**, 030601 (2014).
- [15] T. M. Hoang, J. Ahn, J. Bang, and T. Li, Nat. Commun. **7**, 12250 (2016).
- [16] T. Li, S. Kheifets, D. Medellin, and M. G. Raizen, Science **328**, 1673 (2010).